Environmental Science Nano

ROYAL SOCIETY OF CHEMISTRY

PAPER

View Article Online
View Journal | View Issue

Cite this: *Environ. Sci.: Nano*, 2022, **9**, 714

Identification and quantification of anthropogenic nanomaterials in urban rain and runoff using single particle-inductively coupled plasma-time of flight-mass spectrometry†

Jingjing Wang,[a] MD Mahmudun Nabi,[a] Mahdi Erfani,[b] Erfan Goharian[b] and Mohammed Baalousha *[a]

Urban rain and runoff are potential sources of anthropogenic nanomaterials (engineered and incidental, ENMs and INMs) to receiving waterbodies. However, there is currently a limited knowledge on the nature and concentration of anthropogenic NMs in urban rain and runoff and the current study aims to fill this knowledge gap. Runoff samples were collected from drainage outlets of two bridges (Quail Lane and Blossom Street) in Columbia, South Carolina, representing small and medium size bridges at different times over the duration of precipitation events. Rain samples were collected in the vicinity of the same bridges at the same time as the runoff. Two soil samples at depths of 0 to 3 and 3 to 15 cm were collected at each runoff sampling site to extract background natural NMs. The elemental composition of NMs in the rain, runoff, and soils were determined using single particle-inductively coupled plasma-time of flight-mass spectroscopy (SP-ICP-TOF-MS). Nanomaterials were sorted into groups of similar elemental composition and compared among samples using a two-stage agglomerative hierarchical clustering. Several classes of anthropogenic NMs were identified in the urban rain and runoff, including iron, vanadium, titanium, barium, zinc, copper, chromium, tungsten, antimony, tin, and lead-bearing NMs, most likely due to traffic-related emissions. The total concentrations of anthropogenic titanium and tungsten were estimated using mass balance calculations, total Ti and W concentrations, and shifts in the elemental ratios of Ti/Nb and W/U above the natural background ratios. The concentrations of anthropogenic Ti- and W- in Blossom Street and Quail Lane bridges runoff ranged from 6.0 ± 2.1 to 60.6 ± 0.8 μg Ti L^{-1} and 1.9 ± 0.7 to 20.2 ± 1.8 μg Ti L^{-1}, and 0.23 ± 0.02 to 0.66 ± 0.03 μg W L^{-1}, and 0.11 ± 0.01 to 0.38 ± 0.03 μg W L^{-1}, respectively. Additionally, anthropogenic Ti and W concentrations generally decreased with time following the start of the storm events and increased with increases in traffic density. The detection of anthropogenic NMs in rain implies their occurrence in the atmosphere and thus a potential human exposure/risk *via* inhalation. The direct discharge of anthropogenic NMs to surface water with urban runoff implies exposure and potential risks to aquatic organisms.

Received 12th September 2021,
Accepted 2nd January 2022

DOI: 10.1039/d1en00850a

rsc.li/es-nano

Environmental significance

Identification and quantification of anthropogenic (engineered and incidental) metal-containing nanomaterials in environmental systems are essential to improve the understanding of the nature and magnitude of exposure, environmental fate, and risk assessment of these materials. Single particle-inductively coupled plasma-time of flight-mass spectrometer (SP-ICP-TOF-MS) is a promising tool in the nano-analytical toolbox. However, extracting useful information from the large datasets generated by SP-ICP-TOF-MS remains challenging. This study presents different approaches to extract valuable information from SP-ICP-TOF-MS data in order to differentiate anthropogenic *vs.* natural nanomaterials within urban rainwater and runoff, including the relative abundance of single-metal and multi-metal nanomaterials (smNM *vs.* mmNMs) in the samples of interest compared to reference soil samples and clustering analysis of mmNMs. Anthropogenic NMs identified in urban rainwater and runoff include Ti, Ba, Zn, Cu, Cr, W, Fe, Sn, Sb, Pb, and V-bearing NMs. The concentration of these NMs increased with traffic density and at rush hours. The occurrence of anthropogenic NMs in rain indicates their presence in the atmosphere and potential human exposure through inhalation. The occurrence of anthropogenic NMs in rainwater and runoff indicates exposure of aquatic organisms in receiving surface waters.

[a] *Center for Environmental Nanoscience and Risk, Department of Environmental Health Sciences, Arnold School of Public Health, University of South Carolina, SC 29208, USA. E-mail: mbaalous@mailbox.sc.edu*

[b] *Department of Civil and Environmental Engineering, University of South Carolina, SC 29208, USA*

† Electronic supplementary information (ESI) available. See DOI: 10.1039/d1en00850a

1. Introduction

The rapid growth of the global population and urbanization leads to increased releases of pollutants into the atmosphere, including engineered and incidental nanomaterials (ENMs and INMs, intentionally synthesized and unintentionally generated nanomaterials as a byproduct of other activities, respectively, nanomaterials being particles within the size range of 1–100 nm),[1] which deposit on surfaces *via* dry and/or wet deposition.[2,3] Rain washes gaseous, organic, inorganic, and particulate pollutants released into the atmosphere and deposited on impervious surfaces into surface waterbodies.[4–6] The volume of urban runoff generated annually in the United States is equivalent to the volume of treated wastewater and is estimated at 38 112 billion liters.[7] Unlike sewage and wastewater, in most cases urban runoff enters public waters without any treatment resulting in a direct discharge of pollutants to receiving waterbodies.[8] As a consequence, urban runoff has been recognized as an important cause of water quality impairment related to human activities in ocean shoreline water, the second leading cause of water impairment in estuaries, and the fourth leading cause of water impairment in lakes across the United States.[8] While there has been considerable research into identifying and quantifying organic and metal contamination in urban runoff, less effort has been devoted to evaluating the nature and concentrations of ENMs and INMs in urban rain and runoff.[2,9–11]

In urban areas, anthropogenic NMs, including ENMs and INMs, originate from numerous emission sources, including construction sites, industrial activities, roads, and traffic.[12–14] Road dusts accumulated on impervious surfaces are an important non-point pollution source in urban environments.[9] Road dust can be highly polluted with metal-bearing particles due to traffic-related emissions such as exhaust emissions (V, Ca, Mn, Fe, Cu, Ni, Zn, Cr, Ba, Ce, Al, Co, and PGE)[15–17] and non-exhaust emissions due to wear and tear of vehicle parts such as brake pads (Fe, Mn, Ti, Cu, Ba, Zn, Zr, Cr, Ni, Cd, Sb, Sn, W, and Pb),[18–21] tires (Zn),[22] re-suspension of dust (Al, Si, Ti, Fe, Mn, V, Rb, As),[21] and erosion of road paint marking (Cr, Pb, and TiO_2).[2,10,23] It is worth noting that ENMs (*e.g.*, cerium, aluminum, iron, cobalt, and titanium oxide) are used as fuel additive to enhance fuel efficiency and reduce exhaust emissions[24–27] and TiO_2 particles are widely used as pigments in road marking and paints,[28] resulting in the release of these particles into the road environment. Whereas high concentrations of TiO_2 particles has been detected in urban runoff, CeO_2 particle concentrations remain undetected in appreciable concentrations in urban runoff.[2,29] As exhaust emissions control becomes stricter, relative contributions of non-exhaust sources to traffic-related emissions are expected to dominate particulate matter (PM_{10}) emissions in cities in the near future.[30,31] Among non-exhaust emissions, brake wear is a significant metal and NM contributor, particularly within areas with high traffic density and braking frequency.[18] Brake wear can contribute up to 55% by mass to total non-exhaust traffic-related PM_{10} emissions and up to 21% by mass to the total traffic-related PM_{10} emissions in the urban environment.[18] Road traffic was also found to be a significant contributor to ultrafine particles/NMs (<0.1 μm) where approximately 37, 50, 28, 24, 64, 38, and 22% by mass of Ag, Cd, Cr, Ni, Pb, Sb, V, and Zn, respectively, were found in the ultrafine/NM size range.[32] Consequently, traffic in densely populated areas may elevate some trace elements in both wet and dry deposition locally.[33] Several studies have reported significant levels of metals in runoff from urban areas, especially in highway runoff.[34,35]

Identifying and quantifying the concentrations of anthropogenic NMs (*e.g.*, ENMs and INMs) in environmental systems remain challenging because of the low concentrations of ENMs and INMs compared to the high background concentration of natural NMs (NNMs, *i.e.*, nanomaterials made by nature through biogeochemical or mechanical process without direct or indirect connection to human activity or anthropogenic processes) with similar physicochemical properties such as size, shape, and elemental composition[36–38] and limited methodologies available to accurately identify and quantify ENMs and INMs *vs.* NNMs with sufficient specificity and sensitivity. Among the most promising advancements in this area are the identification of elemental ratios (*e.g.*, Ti/Nb and Ce/La) that can be implemented to quantify the total concentrations of TiO_2 and CeO_2 ENMs and INMs above the natural background concentrations,[2,10,29,39,40] and the use of single particle-inductively coupled plasma-time of flight-mass spectrometer (SP-ICP-TOF-MS) to differentiate ENMs and INMs *vs.* NNMs at the single particle level based on differences in their elemental compositions.[41] These two approaches have their own advantages and limitations. The bulk elemental ratio approach allows the estimation of the total anthropogenic metal concentration, but does not provide information on particle size which can be overcome by fractionating the sample prior to analysis.[2,29] SP-ICP-TOF-MS provides information on particles with masses greater than the method mass detection limit, but requires particle extraction with typically low extraction efficiency.[42,43]

SP-ICP-TOF-MS measures all metal/metalloids in a single particle simultaneously and analyzes thousands of particles in a few minutes. Thus, SP-ICP-TOF-MS generates a large amount of data of NM elemental composition. Extracting useful information from such large datasets remains challenging. Different approaches have been implemented to analyze big-data generated by SP-ICP-TOF-MS, including number concentration and mass distribution of NMs,[44] elemental ratios at the single particle level,[40,45] supervised machine learning,[41] and non-supervised machine learning (*e.g.*, hierarchical clustering).[46] Significant attention has been given to the identification of anthropogenic multi-metal nanomaterials (mmNMs).[40,41,45,46] However, identifying anthropogenic single metal NMs (smNMs) based on SP-ICP-TOF-MS has been largely overlooked because more information is needed to achieve this goal.[46] This study addresses the abovementioned knowledge gaps by combining

mass balance calculations and increases in elemental ratios (*e.g.*, Ti/Nb and W/U) in urban rain and runoff above natural background elemental ratios to quantify the total anthropogenic elemental concentrations, non-target analysis of a large number of individual NMs using SP-ICP-TOF-MS to determine their elemental composition at the single particle level, clustering analysis to classify NMs into groups/clusters of NMs of similar elemental compositions, and comparing the elemental compositions of NM clusters in contaminated urban rain and runoff to a non-contaminated soil to identify anthropogenic NMs in the contaminated samples. Therefore, the aims of this study are to 1) identify classes of anthropogenic NMs and 2) quantify the total concentration of selected anthropogenic metals (*e.g.*, Ti and W) in urban rain and runoff.

2. Materials and methods

2.1. Sampling

Urban rain and runoff were collected from two sites (Blossom Street Bridge and Quail Lane Bridge) within the city of Columbia, South Carolina. Blossom Street (BS) has a four-lane bridge located in the downtown area of Columbia (33°59′15.2″ N, 81°02′53.5″ W) with a medium annual average daily traffic (AADT) density of 22 900 in 2020.[47] The bridge also has two bicycle lanes and two pedestrian lanes. This bridge has fifty-three drainage outlets along each side of the 280 meter-long bridge which collectively collect stormwater and other materials and fluids from the surface and drain to Congaree River. The bridge is located in a mixed commercial and residential area. Quail Lane (QL) Bridge is a two-lane bridge located in a residential neighborhood and runs over Gills Creek (34°00′38.7″ N, 80°57′36.4″ W). The bridge is 20 meters long with twelve 13 cm internal diameter drain tubes on each side. Quail Lane Bridge has a low AADT, estimated to be 1000 in 2019.

Runoff was collected from Quail Lane on October 19, 2019, after 4 sunny dry days, during a rain shower in Columbia, SC (Table S1†) and from Blossom Street Bridge on May 18, 2020, after 17 sunny dry days, during a rain shower in Columbia, SC following the same sampling protocol. Rain was collected in a clean 4 L beaker which was placed 2 feet away from the bridge with no cover or shelter. The precipitation paused for about an hour during sampling (after BS8, 16:15–17:25), so two rain samples were collected for near Blossom Street: the first was collected between 14:05 and 16:15 and the second was collected between 17:25 and 18:35. Runoff was collected from the bridge's drainage outlets in a clean acid-prewashed 5 gallon HDPE bucket (Letica Corporation, Rochester, MI) during different times of the rain event (see Table S1†). Samples were transferred into 1 L or 250 mL acid-washed HDPE bottles (VWR, Radnor, PA). Between samples, the bucket was rinsed with water to eliminate any possible contamination. All samples were stored at 4 °C after collection until further processing and analysis within few days following sampling.

Soil samples were collected at two different depths (0 to 3 cm and 3 to 15 cm) near the runoff sampling sites (Blossom Bridge and Quail Lane) to extract background natural nanomaterials and to account for potential topsoil contamination. A third top soil sample (CCAL, 0–15 cm) was collected from Dillon County (34°30′15.8″ N, 79°25′23.3″ W) South Carolina, a distant site from the two Bridges to account for potential topsoil contamination at the two Bridges' sampling site. The topsoil is characterized as a dark grayish brown loamy sand with a weak fine granular structure.[48] The soils were collected using a soil auger (AMS, American Falls, ID). All soils were dried in an oven at 110 °C overnight and sieved through a 2 mm acid-cleaned nylon sieve (Zhangxing Instrument, Shanghai, China). The <2 mm fractions were stored at −20 °C freezer before extraction as described below. The elemental composition of the NMs extracted from CCAL, 0–15 cm soil were compared to those extracted from soils collected near the sampling sites to account for any potential contamination near the sampling site. The elemental composition of the five soils were very similar (see section 3.2.2) indicating the absence of anthropogenic contamination of soil NMs.

2.2. Total elemental concentration

The elemental concentrations in bulk rain and runoff samples were determined using Perkin Elmer NexION 350D ICP-MS (PerkinElmer Inc., Waltham, MA, USA) following total digestion using 30% H_2O_2, distilled HF, and HNO_3 (Fisher Chemical, Fair Lawn, NJ, USA) as described in the ESI† section and elsewhere.[2,40] At the end of the digestion, digestates were reconstituted in 1% HNO_3 for ICP-MS analysis. The calibration standards (0.001 to 100 μg L^{-1} in 1% HNO_3) were prepared by mixing three different commercially available standards (ICP Complete Group Calibration Standard, ICP Refractory Element Group Calibration Standard, and ICP Internal Element Group Calibration Standard, BDH Chemicals, Radnor, PA, USA). The ICP-MS was tuned for maximum sensitivity before each analysis. The ICP-MS operating parameters are presented in Table S2.†

2.3. Single particle analysis

Single particle analysis of NM extracted from rain, runoff samples, and reference soils were performed using an ICP-TOF-MS (TOFWERK, Thun, Switzerland) to determine all isotopes within a single particle simultaneously.[49] Samples were prepared following the protocol used in previous studies and described in detail in the SI section.[48] Briefly, runoff samples were bath sonicated (Branson 2800, 40 kHz, Danbury, CT, USA) to disrupt microaggregates, then the <1 μm particles were separated by centrifugation (Eppendorf, 5810R, Hamburg, Germany). Soils were mixed with UPW at pH 7 overnight, followed by sonication to disperse NNMs and centrifugation to separate particles <1 μm. The instrument operating parameters and the monitored isotopes are summarized in the ESI† (Tables S3 and S4, respectively). Mass spectra calibration and tuning

were performed on icpTOF daily to optimize the instrument conditions for maximum sensitivity with a multi-element tune solution (iCAP Q/RQ Tune Solution, Thermo Scientific, Ward Hill, MA, USA). Transport efficiency was calculated *via* the known size method using a certified 60-nm Au ENMs (NIST RM 8013 Au, Gaithersburg, MD, USA) and a series of ionic Au standards (BDH Chemicals, West Chester, PA, USA).[50] Dissolved calibration standards were prepared from a mixed multi-element ICP certified reference standard (0, 1, 2, 5, and 10 μg L^{-1}, diluted in 1% HNO_3, BDH Chemicals, Radnor, PA, USA) to determine the elemental specific mass responses of particles. A 4.5% H_2/He gas mixture was used as collision gas to eliminate/minimize interferences and was optimized for $^{56}Fe^+$ and $^{28}Si^+$ signals. All samples were diluted (10–20 folds for rain, 100–500 folds for runoff, and 5000 folds for soil extracts) with UPW prior to analysis to avoid coincidence and eliminate dissolved background. All samples and UPW blanks were prepared and analyzed in triplicates. The SP-ICP-TOF-MS measures all isotopes (mass range of 14–275 amu) simultaneously at a sampling rate of 33 KHz. However, mass spectra were pre-averaged before readout, resulting in an integration time of 2 ms. Data was acquired for 200 s for each replicate. The data was combined for the three replicates to achieve comprehensive analysis due to limited detection events of certain elements. All data processing – particle/baseline signal separation and elemental mass calculation – were performed using Tofware as described elsewhere.[40,51] The mass and size detection limits assuming pure metal and metal oxide phases are summarized in Table S4.†

2.4. Clustering analysis of SP-ICP-TOF-MS data

SP-ICP-TOF-MS generates large datasets of the elemental composition (*e.g.*, masses of metals/metalloids in a single particle) of tens of thousands of NMs in each sample, which requires an automated and robust big-data processing approach to reduce the SP-ICP-TOF-MS large data files to a reportable format that can be used to extract elemental fingerprint information of NMs. Detected NMs were classified into single- and multi-metals (smNMs and mmNMs). The smNMs were considered as their own clusters because the NM mass and number concentrations are not sufficient to cluster smNMs. The mmNMs were classified into clusters of NMs of similar elemental composition with an unsupervised data analysis approach (agglomerative hierarchical clustering[52]) using MATLAB, to identify clusters/groups of NMs of similar elemental composition and to identify their mean elemental composition, with the aim to identify anthropogenic NMs in the different rain and runoff samples. The mmNMs were processed through a two-stage (*e.g.*, intra- and inter-sample) agglomerative hierarchical clustering analysis following our previously developed two-stage clustering method.[48]

First, intra-sample clustering was performed on all metal masses in each NM to generate clusters that best account for variance in NM elemental composition in each sample. The dissimilarity matrix was constructed by calculating the pairwise correlation distance between NMs based on elemental mass. The pairwise correlation distance represents the similarity/dissimilarity of NM composition to one another. A small correlation distance indicates a high similarity of the elemental composition of two NMs and *vice versa*. After the correlation distance between all NMs was calculated, agglomerative hierarchical clustering was performed using average correlation distance method. This step generated a unique cluster dendrogram for each sample, which was divided into major clusters using a specified correlation distance cutoff. The distance cutoff of 0.5, was determined by visually inspecting the dendrogram and through trial and error in order to minimize the variance/diversity in NM elemental composition in the major clusters. Then, a cluster representative was identified for each major cluster as the mean of metal masses in individual NMs within each cluster taking into account all elements that occurred in at least 5 percent of NMs within the cluster.

Second, inter-sample clustering was performed on the major cluster representatives identified in the intra-sample clustering to group/cluster the similar NM major clusters identified in the different samples. The intra-sample clustering was performed using the same agglomerative hierarchical clustering method described above. This step generated a cluster dendrogram for intra-sample cluster representatives, which was divided into major clusters using a distance cutoff of 0.2, as performed for the intra sample clusters.

The mean intra-sample cluster composition was determined as the mean of metal mass fraction in all NMs in the cluster and was compared across samples. The mass fraction of a given metal in each NM was determined as the mass of that metal divided by the sum of masses of all metals in that NM. Because all samples originate from the same source for each sampling site, the mean of all mean intra-sample cluster composition was calculated for each second stage major cluster, and a heat map was generated to interpret the data and visualize cluster composition. Selected elemental ratios were determined on a particle-by-particle basis for all NMs containing the select elements. The number concentration (NM mL^{-1}) of the total, smNMs, mmNMs, and cluster members were determined according to the single particle theory.[50] Finally, heat maps were generated by comparing the number concentration of NMs in each major cluster among the different samples. Furthermore, clusters of interest (*e.g.*, Fe cluster here) were clustered again to identify sub-clusters that might have a high content of the major element and relatively low content of the minor or trace elements. In this case, the distance cutoff for the first and second stage clustering were 0.05 and 0.2.

2.5. Anthropogenic Ti and W concentration

The concentrations of anthropogenic Ti and W were calculated using mass balance calculations and shifts in bulk elemental

ratios (Ti/Nb and W/U). The natural background elemental ratios of Ti/Nb has been illustrated elsewhere.[2,10,29,39,40] Because W is one of the most incompatible elements during mantle melting, a concentration ratio involving W and other similarly incompatible elements (*e.g.*, W/Ba, W/Th, or W/U) can be used to differentiate natural from anthropogenic W.[53–58] The natural background elemental ratios of W/U, W/Th, and W/Ba were calculated from W, U, Th, and Ba concentrations obtained from a spatially balanced array of 4857 soil samples across the Conterminous United States that were obtained from the United State Geological Survey (USGS) publication (Fig. S1†).[59] The elemental ratios distributions of W/U, W/Th, and W/Ba for all soil samples across the United States as well as South Carolina are presented in Fig. S1 and S2.† The mean elemental ratios of W/U, W/Th, and W/Ba in South Carolina are 0.26 ± 0.17, 0.07 ± 0.05, and (0.56 ± 0.41) × 10^{-2}, respectively (Fig. S1 and S2†). These values were used to estimate the total anthropogenic tungsten contamination in the rain and runoff samples. Due to the co-contamination of urban rain and runoff with W and Ba (see Results and discussion), W/U was selected as the elemental ratio to quantify anthropogenic W concentration.

3. Results and discussion

3.1. Elemental concentrations

Substantial bulk metal concentrations (*e.g.*, 2 to 28 μg Ti L^{-1}, 13 to 315 μg Fe L^{-1}, 1 to 7 μg Cu L^{-1}, and 8–70 μg Zn L^{-1}) were detected in the three rain samples (Fig. 1, Tables S5 and S6†). This is because washout (below cloud scavenging) is a major mechanism by which atmospheric contaminants are incorporated in rainfall.[5,60,61] The composition of rain reflects that of the atmosphere through which it falls and consists of a mixture of natural (*e.g.*, soil dust) and anthropogenic (*e.g.*, industrial and vehicular emissions) chemicals.[62,63] Metals of dominantly crustal origin (Fe, Al) constitute the largest fraction of the total metal content in rain, accounting for >75% of the analyzed metals. Other than Al and Fe, rain contained high concentrations of metals, such as Sn, Ti, Zn, Mn, Ba, and Cu, suggesting contamination with traffic-related emissions. Elevated Zn and Cu in rain have been attributed to vehicular emission in urban environments.[13] Tungsten concentrations were higher than those of heavy rare earth elements despite their similar abundance in the upper crust (*e.g.*, W = 1.9 ppm, Eu = 2.3 ppm, Yb = 1.96 ppm),[64] indicating a potential anthropogenic contribution of W in rain. The higher metal concentrations in the second rain sample (17:25 to 18:35) in Blossom Street compared to the first rain sample (14:05 to 16:15) indicates increased metal emission and washing overtime, possibly due to increased traffic density during the peak traffic time in Columbia, South Carolina.

For each sampling site, metal concentrations were generally higher in the runoff compared to rain (Fig. 1, Tables S5 and S6†), suggesting that road dust is a significant contributor to metal contamination in urban runoff. Stormwater runoff typically washes off contaminants deposited (dry deposition) on impervious surfaces and top soils, some of which may have accumulated high concentrations of metals (*e.g.*, Pb, Zn, Cu, and Cd), to receiving surface waters.[65] Metal concentrations were highest in the first runoff sample and trended lower with time, suggesting depletion of the metal source on urban surfaces. The concentrations of metals in the runoff followed the same pattern as in the rain with Al and Fe displaying the highest concentrations followed by Sn, Ti, Zn, Mn, Ba, and Cu. These metals are indicators of traffic-related emissions. This is in agreement with previous studies where Zn was found in the highest concentration in bridge runoff followed by Ba, Cu,

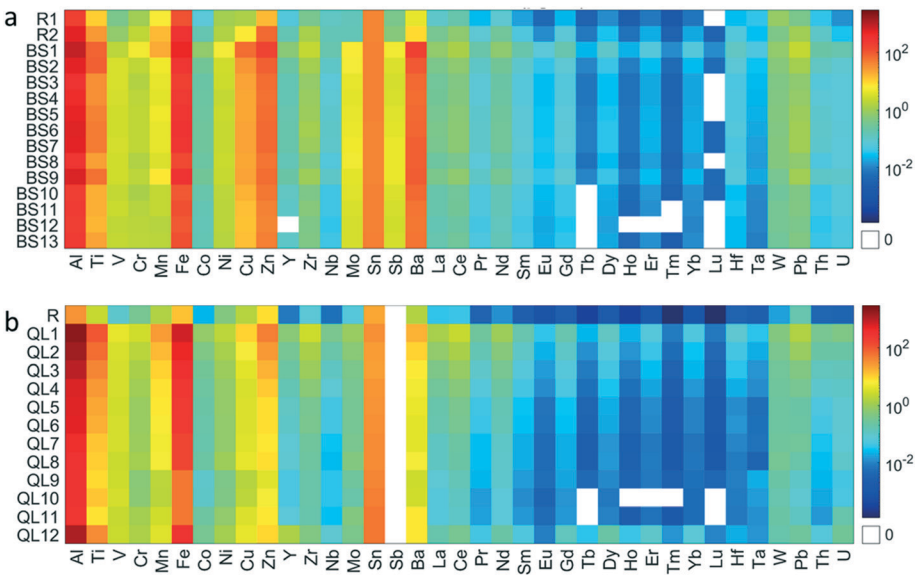

Fig. 1 Heat map of the bulk total metal concentrations (μg L^{-1}) in rain and runoff in (a) Blossom Street and (b) Quail Lane. R, R1, and R2 refer to rain samples. Sb was not measured in Quail Lane samples.

and Pb.[66] Al, Ti, and Fe can be attributed to both natural (soil) and anthropogenic emissions (*e.g.*, road marking, car paint, brake pads, and other vehicular parts, *etc.*).[67,68]

Metal concentrations (*e.g.*, Cr, Ni, Cu, Mo, Ba, and W) were higher in Blossom Street rain and runoff than in Quail Lane rain and runoff (Fig. 1, Tables S5 and S6†), which can be attributed to the higher traffic density on Blossom Street Bridge compared to Quail Lane Bridge. Previous studies demonstrated that metals such as Fe, Ba, Zn, Cu, Sb, Sn, and Pb were higher in city/heavy traffic/industrial rainwaters compared to suburban sites' rainwater.[67,69]

Metals in urban runoff are associated mainly with anthropogenic particles, including INMs and ENMs.[70] While there has been considerable work on the characterization of metal contamination in urban runoff,[71] little attention has been given to identifying the elemental composition of metal bearing NMs and to differentiate natural *vs.* incidental and engineered NMs. Below we discuss the identification of anthropogenic NMs in urban rain and runoff using SP-ICP-TOF-MS and agglomerative hierarchical clustering analysis.

3.2. Identification of incidental nanomaterials using SP-ICP-TOF-MS

3.2.1. Particle number concentration and size (mass) distribution. All monitored elements were detected in urban rain and runoff as single particles at concentrations higher than the number concentration detection limit (Fig. 2 and Table S4†). Similar to our previous study,[48] all elements – Si and Fe more frequently than other elements – were detected as single particles in the blanks at low concentrations (Table S4†). Most of the detected particles in the blanks were smNMs. In contrast, mmNMs were rarely detected in the blanks, suggesting that all mmNMs are true particles.[48]

The number concentrations of metal containing particles were generally higher in Blossom Street rain and runoff compared to those in Quail Lane (Fig. 2), consistent with the total metal concentrations trend. Fe, Al, Si, Ti, Mn, and W-bearing NMs displayed the highest number concentration in the runoff samples. The high number concentrations of Fe, Al, Si, Ti, and Mn-rich NMs is expected given that they are the dominate naturally occurring particles in soils.[48] Surprisingly, W displayed high number concentrations in the rain and runoff samples, indicating a potential anthropogenic W contamination. W is a rare element in the earth crust and its abundance (*e.g.*, 1.9 ppm) is similar to that of heavy rare earth elements (*e.g.*, europium – 2.3 ppm, ytterbium – 1.96 ppm).[64] Yet, W particle number concentration was orders of magnitude higher that these heavy rare earth elements in urban rain and runoff (Fig. 2). Most elements exhibited higher number concentrations in the urban runoff than in the rain.

The mass ranges of NMs in representative rain, runoff, and soil samples are presented in Fig. S3–S5,† respectively. For each element, the mass distributions are similar across the soil, rain, and runoff samples. The corresponding size

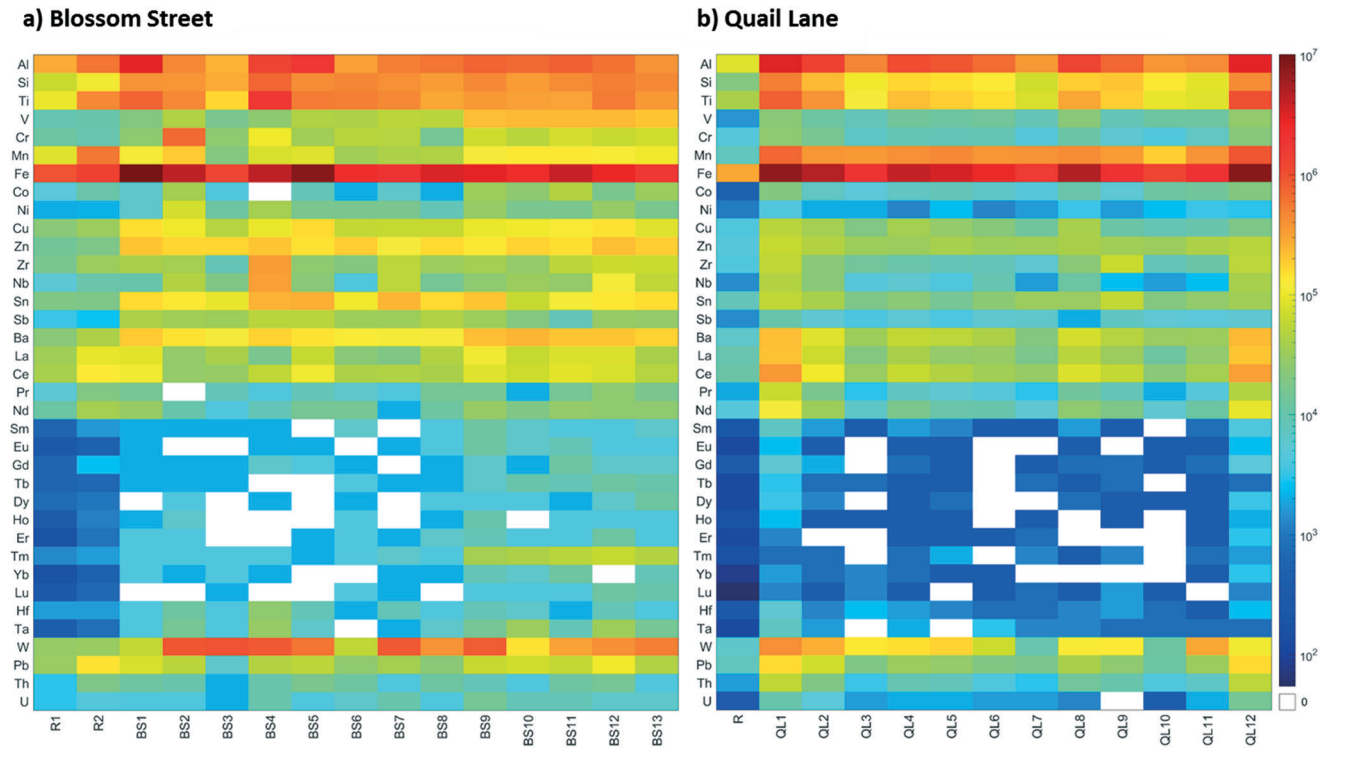

Fig. 2 Heat map of the number concentration (particle mL^{-1}) of elements detected in urban runoff samples (a) Blossom Street (BS) bridge runoff and (b) Quail Lane (QL) bridge runoff. R, R1, and R2 refer to rain samples.

distributions of the detected NMs assuming pure metal and metal oxide particle phases are presented in Fig. S6–S8.† The percentage of the nanosized particles (*e.g.*, <100 nm) relative to the total number of detected particles is presented in Fig. S9–S11.† For all elements, except Al, Si, and in some samples Ti, the majority of the detected particles were within the NM size range.

The detected NMs by SP-ICP-TOF-MS can be classified as either smNMs or mmNMs (Fig. S12 and S13†). Al, Zr, Nb, La, Ce, Pr, Nd, Hf, Ta, Pb, and Th-bearing NMs occurred dominantly as mmNMs in rain, runoff, and soils, indicating a common dominant, likely natural source of these NMs. In contrast, whereas V, Zn, Sn, Sb, and W-bearing NMs occurred dominantly as smNMs in the Blossom Street and Quail Lane urban runoff – Ba-bearing NMs also occurred dominantly as smNMs in Blossom Street runoff only –, they occurred dominantly as mmNMs in rain and soil samples, suggesting that V, Zn, Sn, Sb, Ba, and W smNMs in urban rain and runoff might be driven by anthropogenic inputs. Other elements such as heavy rare earth elements were detected at low frequency for which it was not possible to discern a specific patterns.

3.2.2. Identification of multi-metal NM clusters. For each sample, mmNMs were clustered into 30 clusters (Fig. S14†), including Al, Si, Fe, Mn, Cu, Zn, Ce, Sn, Sb, Zr, Th, W-bearing NM clusters. A distance cutoff of 0.5 was selected to group these clusters into major clusters, while preserving the identity of most of the clusters. Consequently, 5 to 14 major mmNM clusters were identified in each sample (Fig. S14†). Inter-sample clustering generated 21 clusters in Blossom Street and Quail Lane runoff and 15 clusters in the soil NNMs using a distance cut-off of 0.2 (Fig. S15†). A cutoff of 0.2 was selected to avoid grouping clusters of different elemental compositions into major clusters. The elemental composition (mean mass fraction of metals) of the identified clusters across all samples is presented in Fig. 3 and S16,† for the mean mass fraction of major second stage clusters across all samples and the individual clusters in the different samples, respectively. Typically, the composition of each cluster is dominated by one metal and contains minor or trace concentrations of other metals. Twelve NM clusters were identified in the five soil samples including Al, Fe, Ti, Si, Ce, Mn, Zr, Ba, Cu, Sn, Zn, Pb-rich NM clusters (Fig. 3 and S16†), typical of NNMs identified in uncontaminated natural soils.[48] Al, Fe, Ti, Si, Ce, Mn, and Zr–rich NM clusters accounted for >99.7% of the measured mmNMs in all soils. The elemental composition of each of the identified NM clusters in the five soils were similar. These results demonstrate the absence (or the insignificance) of anthropogenic NM contamination in the soil collected near the bridges. Al-, Fe-, Si-, Ti, Ce, Mn, and Zr-rich NM clusters accounted for 94.1 to 99.9% of all mmNMs in Blossom Street and Quail Lane rain and runoff and 98.7 to 99.9% of all mmNMs in Quail Lane rain and runoff. Some clusters such as Al, Si, Fe, Ti, Ce, Zr, Ba, Mn, Dy, and Th-rich NM clusters were identified in rain, runoff, and soil samples, suggesting natural or mixed natural and anthropogenic origin of these NM clusters in urban rain and runoff (Fig. 3 and S16†). Other clusters, such as Sb, Cr, and W-rich NM clusters, were identified in rain and urban runoff only, indicating an anthropogenic origin, most likely traffic-related emissions such as brake pad and tire wear,[72,73] of these NM clusters (Fig. S16†). Furthermore, NM clusters identified in urban rain and runoff displayed a different elemental fingerprints compared to those identified in the soil samples as discussed below.

Al- and Si-rich NM clusters. Al-rich NM cluster accounted for 12 to 82% and 54 to 71% of all mmNMs in Blossom Street and Quail Lane rain and runoff, respectively. Si-rich NM cluster accounted for 9 to 17% and 7 to 20% of all mmNMs in Blossom Street and Quail Lane rain and runoff, respectively. The elemental ratios of Si/Al (*e.g.*, 0–2 and 0–10 for Al and Si-rich clusters, respectively) in the Blossom Street and Quail Lane rain and runoff are similar to those in NNMs detected in soil samples (Fig. 4a–e). However, a fraction (up to 25%) of NM in Si-rich cluster in Blossom Street rain and runoff displays a high Si/Al (*e.g.*, >10) (Fig. 4c). Additionally, W was detected at trace concentrations in Al- and Si-rich NM clusters in Blossom Street and Quail Lane rain and runoff but not in the soil samples (Fig. 3 and S16a and S16b†). These observations suggest a contribution of anthropogenic NMs to these clusters.

Ti-rich NM cluster. Ti-rich NM cluster accounted for 12 to 28% and 0 to 7% of all mmNMs in Blossom Street and Quail Lane rain and runoff, respectively. The elemental ratios of Ti/Fe in Blossom Street rain and runoff were higher (broader distribution and higher fraction of NMs with higher Ti/Fe ratios) than those in Quail Lane rain and runoff and soil samples (Fig. 4f–h), suggesting a higher contribution of anthropogenic origins to this clusters in Blossom Street than Quail Lane. Additionally, Ti-rich NMs in urban rain and runoff show associations with W, Sn, and Cr, which were not observed in the Ti-rich NMs in the soil samples (Fig. 3 and S16c†), further confirming the anthropogenic origin of these NMs.

Fe-rich NM cluster. Fe-rich NM cluster accounted for 23 to 69% and 10 to 22% of all mmNMs in Blossom Street and Quail Lane runoff, respectively. Fe cluster shows elemental associations (*e.g.*, Ti, Mn, Al, Ba, Ce, Zr, Pb, La, Pr, Fig. 3 and S16d†) which are typical of natural elemental associations in Fe-rich NNMs[48] and these Fe-metal associations were present across rain, runoff, and soil samples. The Fe cluster also displays associations with W, Cr, Cu, Sn, Zn, Ni, Sb, and Co in the rain and runoff only, suggesting anthropogenic contributions, most likely traffic-related emissions such as brake pads and tire wear,[72,73] of NMs containing these elemental associations.

The clustering of NMs in the original sample is driven largely by the major elements within NMs and may hide subtle differences between NMs with the same mass of the major elements but small amount of different minor/trace elements. Thus, the iron cluster was re-clustered to identify

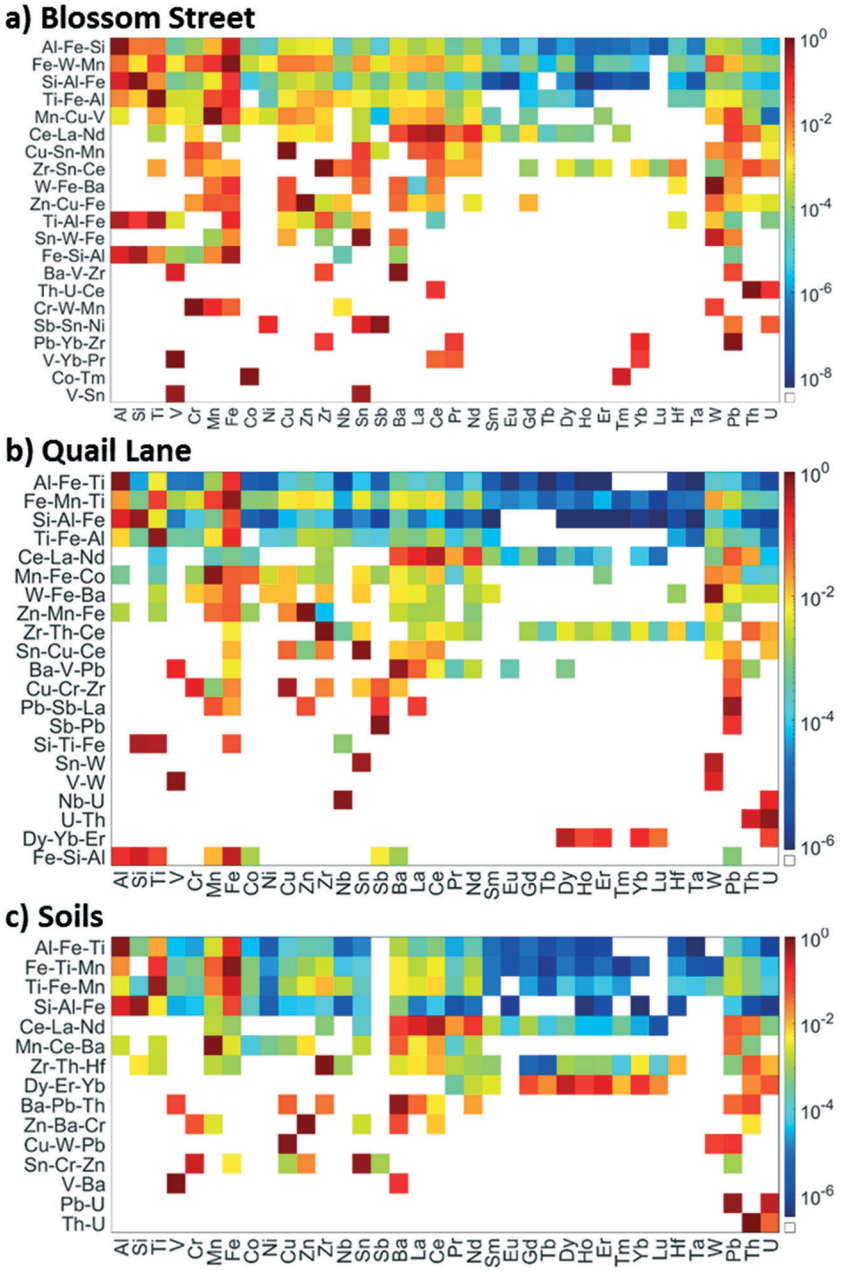

Fig. 3 Elemental composition (mass fraction) of all multi-metal nanomaterial (mmNM) clusters identified in: (a) Blossom Street bridge runoff, (b) Quail Lane bridge runoff, and (c) soils. The values represent the mean mass fractions of elements in clusters identified in the different samples. Elemental composition for each cluster in each sample is presented in Fig. S16.† Distance cutoff for the first and second stage clustering were 0.5 and 0.2, respectively.

such subtle differences (Fig. 5 and S17†). Several sub-clusters were identified in the Blossom Street and Quail Lane runoff that were not identified in the soil samples, including $Fe_{0.49}Cr_{0.48}Mn_{0.03}$, $Fe_{0.49}Cu_{0.49}Mn_{0.004}$, $Fe_{0.58}Zn_{0.38}Ti_{0.01}$, $Fe_{0.56}W_{0.4}Cr_{0.03}$, and $Fe_{0.34}Sn_{0.33}Cu_{0.18}$ (the subscript numbers refer to the mean mass fraction of each element within NMs). Chromium and iron are major elements found in the composite materials in motor vehicles including brake pads, and thus, are expected to be observed in rain and urban runoff.[74] The Cr/Fe ratio was higher in rain and runoff samples compared to those in the soil samples (Fig. 4i–k), suggesting an anthropogenic origin of Fe–Cr- bearing NM in rain and runoff. Additionally, many Fe-clusters in the urban runoff contained NMs associated with W which were not observed in the soil samples.

W NM cluster. In the detected W-bearing mmNMs, W occurred as the major element accounting for >83% of the total metal mass within individual NMs, and it was associated with Mn, Fe, Cu, Sn, Ba, La, Ce, Hf, and Pb (Fig. 3 and S16e†). W also occurred as a minor element in Fe, Al, Si,

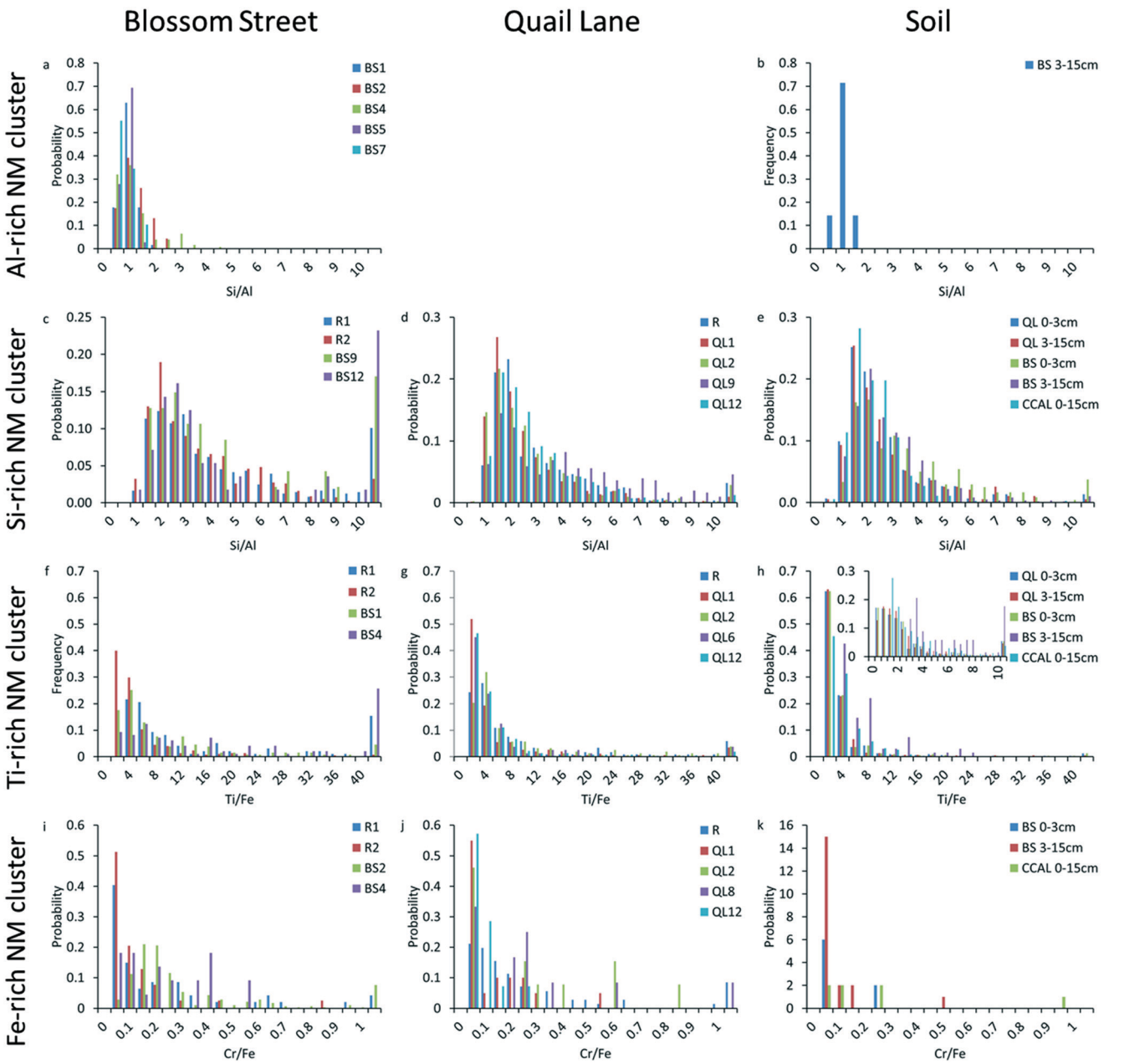

Fig. 4 Elemental ratios in a select set of mmNM clusters: (a and b) Si/Al in Al-rich NM cluster, (c–e) Si/Al in Si-rich NM cluster, (f–h) Ti/Fe in Ti-rich NM cluster, (i–k) Cr/Fe in Fe-rich NM cluster. R: rain, BS: Blossom Street, QL: Quail Lane. The Si/Al in the Al-rich particle cluster in Quail Lane is not presented as there were few mmNMs containing Si and Al in this mmNM cluster.

Ti, Mn, Zr, Sn, Zn, and Cr-rich NM clusters. Sb, Sn, Cu, Zn, Pb, and Cr NM clusters were also identified in urban rain and runoff (Fig. 3 and S16f–S16k†). These clusters contained multiple metals suggesting that they might be metal alloy NMs. Metal alloys are widely used in vehicles including brake pads.[75,76] Mn, Zr, Ce, and Ba NM clusters (Fig. 3 and S16l–S16o†) generally contained few NMs representing <3% of all mmNMs in rain and runoff and therefore were not further investigated.

The number concentration of mmNMs in each cluster is presented in Fig. 6. Fe, Al, Si, and Ti-rich mmNMs display the highest number concentrations and accounted for the majority (>80%) of mmNMs. The number concentrations of anthropogenic mmNMs such as Cu, W, Zn, Sn, Sb, Cr, Pb-rich NMs are relatively small and accounted for <6% of the total number of mmNMs. Nonetheless, most clusters, particularly those identified in Blossom Street rain and runoff, had anthropogenic NM contributions. This is consistent with the composition of road dust, a major contributor to metallic NMs in urban runoff. Road dust primarily consists of soil-derived minerals (60%), organic matter (2%), and the remaining amount from brake and tire wear, combustion emission, fly ash from asphalt, and abrasion of road marking (white and yellow paint).[77] Approximately, 40–50% of the soil-derived minerals are

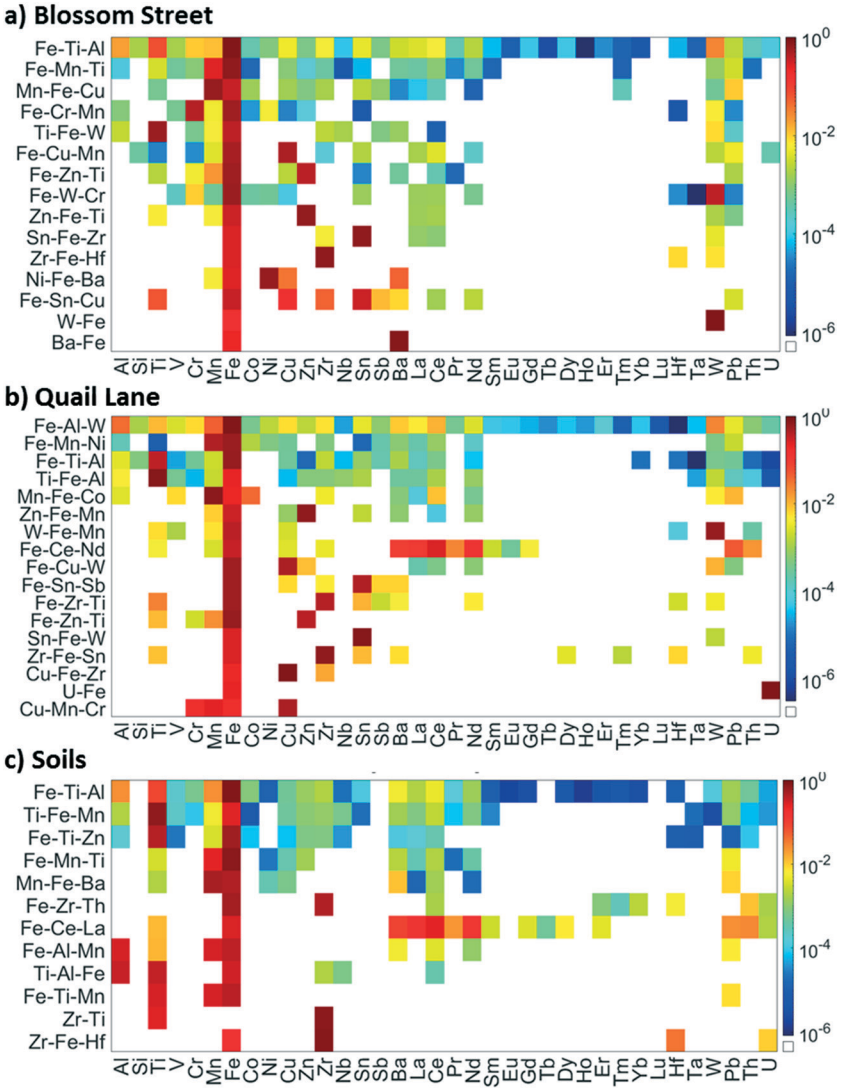

Fig. 5 Elemental composition (mass fraction) of the sub-clusters identified in the iron rich mmNM cluster in: (a) Blossom Street bridge runoff, (b) Quail Lane bridge runoff, and (c) soils. The values represent the mean mass fractions of all clusters identified in the different samples. Elemental composition for each sample is presented in Fig. S17.† Distance cutoff for the first and second stage clustering were 0.05 and 0.2, respectively.

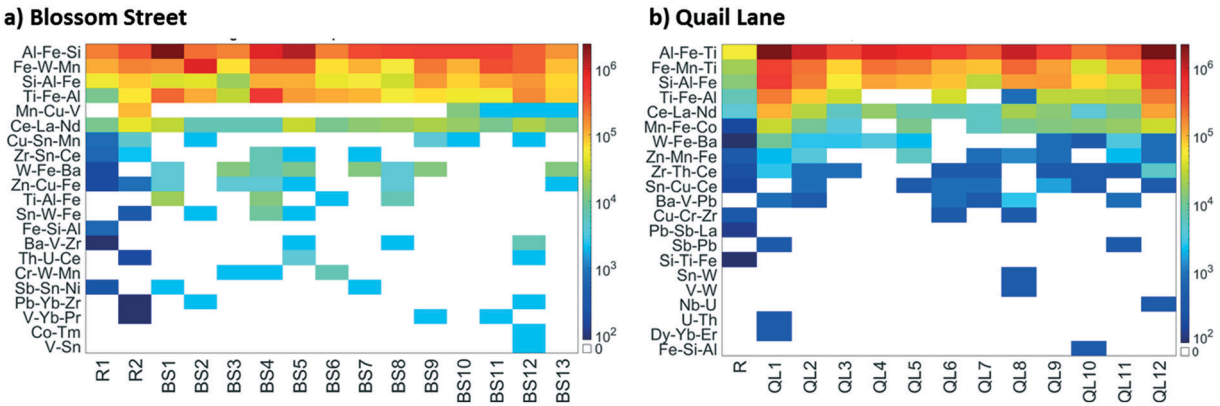

Fig. 6 Heat map of the number concentrations of multi-metal nanomaterials (mmNMs, particle mL^{-1}) in the clusters identified in: (a) Blossom Street bridge and (b) Quail Lane bridge. First and second stage clustering cutoffs were set at 0.5 and 0.2, respectively. R1, R2, and R are rain samples collected at Blossom Street bridge, and Quail Lane bridge, respectively. BS1–13 and QL1–12 are bridge runoff samples collected at different time points during rain events (see Table S1†).

quartz and the remaining amounts are clay-forming minerals such as albite ($NaAlSi_3O_8$), microcline ($KAlSi_3O_8$), chlorite, and muscovite ($KAl_2(Si_3Al)O_{10}(OH)_2$) originating from surrounding soils.

3.3. Concentrations of anthropogenic Ti and W

Ti and W concentrations in Blossom Street rain were higher than those of Quail Lane rain (Fig. S18a and S18b and S19a and S19b†), due to higher traffic density, human activity, and longer dry period. The Ti/Nb ratios in the two Blossom Street rain were 135 ± 3, and 198 ± 7, respectively (Fig. S19c†). These ratios are lower than those of Quail Lane rain, even lower than the natural background ratio (*e.g.*, 266 ± 9),[40] suggesting a possible rain contamination with Nb. Around 80% of the Nb produced worldwide is used as a microalloying element in steels applied in the automotive industry, pipelines, and constructions,[78–80] which could result in Nb contamination in the atmosphere.[81,82] However, the overall volume of Nb used in these applications remain limited compared to the overall volume of TiO_2 used in various applications, such as paint and road marking, in the urban environment.[28] The potential co-contamination of these samples with Nb will lead to the underestimation of the anthropogenic Ti concentration. The Ti/Nb ratio of Quail Lane rain was 392 ± 36, higher than the natural background elemental ratio, indicating contamination of anthropogenic Ti-bearing NMs in the atmosphere (Fig. S19c†). Thus, precipitation results in the wet deposition of anthropogenic Ti-bearing NMs, consistent with the high relative abundance of smTi-bearing NMs in the rain. Rain collected in both locations displays higher W/U than the natural background ratios (Fig. S18d and S19d†), suggesting that the rain samples were contaminated with W, consistent with the identification of W-bearing NM clusters in rain.

Titanium and W concentrations were highest in the first runoff sample and trended lower with time (Fig. S18a and S18b, S19a and S19b†). All bridge runoff samples displayed higher total Ti concentration than the rain samples, indicating that other sources contributed to the total concentrations in the bridge runoff such as NMs deposited on the bridge surfaces. For Blossom Street, Ti/Nb was above the natural background ratio and was highest in the second runoff sample (*e.g.*, 859 ± 17) (Fig. S18c†), then reached a plateau of 482 ± 50. For Quail Lane, the elemental ratio of Ti/Nb was lowest (282.7 ± 11.7) in the bridge runoff at the beginning of the rain event and increased with time (Fig. S19c†), then reached a plateau of approximately 434.4 ± 8.1 after 75 minutes from the start of the storm event. The W/U (Fig. S19d†) followed a similar trend as Ti/Nb. This increase in Ti/Nb and W/U overtime can be attributed to increased emission of anthropogenic Ti- and W-bearing NMs and/or a decreased contribution of naturally occurring Ti- and W-bearing NMs with time due to the depletion of naturally occurring NMs from road surfaces within the first 75 minutes of the storm event.

For Blossom Street, anthropogenic Ti concentration increased from 32.8 ± 4.9 to 60.6 ± 0.8 μg L^{-1} within the first 15 min of the storm event and then decreased and increased over the sampling period (Fig. 7a). For Quail Lane, the anthropogenic Ti concentration increased from 8.4 ± 2.0 to 11.2 ± 0.6 μg L^{-1} within the first 15 min of the storm event and then decreased with time to 1.9 ± 0.7 μg L^{-1} (Fig. 7c). The relatively low Ti concentration in Quail Lane runoff compared to those measured in a previous study is likely because this bridge is a small bridge within a residential area with a low traffic density. The higher anthropogenic Ti concentration in Blossom Street compared to Quail Lane runoff can be attributed to the higher traffic density and longer dry period. It is worth noting that the estimated anthropogenic Ti concentrations in Blossom Street runoff might be lower than the actual concentrations due to a possible Nb contamination in rain and possibly runoff. Anthropogenic W concentrations in the runoff samples generally decreased over time and were at least 20 times lower than anthropogenic Ti concentrations (Fig. 7b–d).

3.3.1. Source of NM contamination in rain and runoff. Multiple lines of evidence point out that traffic emissions, in particular brake pad wear, are the major source of anthropogenic NM contamination in rain and bridge runoff. These pieces of evidence include: 1) the sampling locations, 2) the metals and mmNM elemental composition in rain and runoff, 3) the higher metal contamination in runoff samples from bridge drains compared to rain, 4) the increase in metal and anthropogenic NM concentrations with the increase in traffic density, and 5) the increases in metal mass concentration and NM number concentrations at the peak hour.

The runoff was collected from bridge drains in order to capture metal and NM signatures from traffic-related emissions. Traffic-related emissions include exhaust emissions, such as fuel lubricant combustion, catalytic converters, particulate filter, and engine corrosion (*e.g.*, V, Ni, Zn, and Sb),[15,74,83] and non-exhaust emissions due to wear and tear of vehicle parts such as brake pads (*e.g.*, Fe, Mn, Ti, Cu, Ba, Zn, Zr, Cr, Ni, Cd, Sb, Sn, W, and Pb),[18–21] tires (*e.g.*, Zn),[22] re-suspension of dust (*e.g.*, Al, Si, Ti, Fe, Mn, V, Rb, As),[21] and erosion of road paint marking (Cr, Pb, and Ti).[2,10,23] The concentrations of metals emitted in the exhaust-emissions is very low compared to those emitted from non-exhaust traffic emissions,[30,31] suggesting that non-exhaust emissions drive anthropogenic metal and NM concentrations in rain and runoff. It has been shown that brake and tire-wear account for 48% of Cu and 28% of Zn in urban stormwater, and engine oil contributes <1% of Cu and Zn.[35]

The identified mmNM clusters in rain and runoff (*e.g.*, Sb, Sn, Cu, Zn, Pb, W, Cr-rich NM clusters, and $Fe_{0.49}Cr_{0.48}Mn_{0.03}$, $Fe_{0.49}Cu_{0.49}Mn_{0.004}$, $Fe_{0.58}Zn_{0.38}Ti_{0.01}$, $Fe_{0.56}W_{0.4}Cr_{0.03}$, and $Fe_{0.34}Sn_{0.33}Cu_{0.18}$) are consistent with the elemental and mineralogical composition of brake pad materials and debris. Materials used for brake linings include metallic friction material (Fe and Fe–Cu oxides), lubricants (graphite and Fe–Sb–Mo–Sn–Mn sulfides) and mineral fibers (barite, calcite, zircon, and Al-silicates) used as fillers, as well as other elements (Ti, Cr,

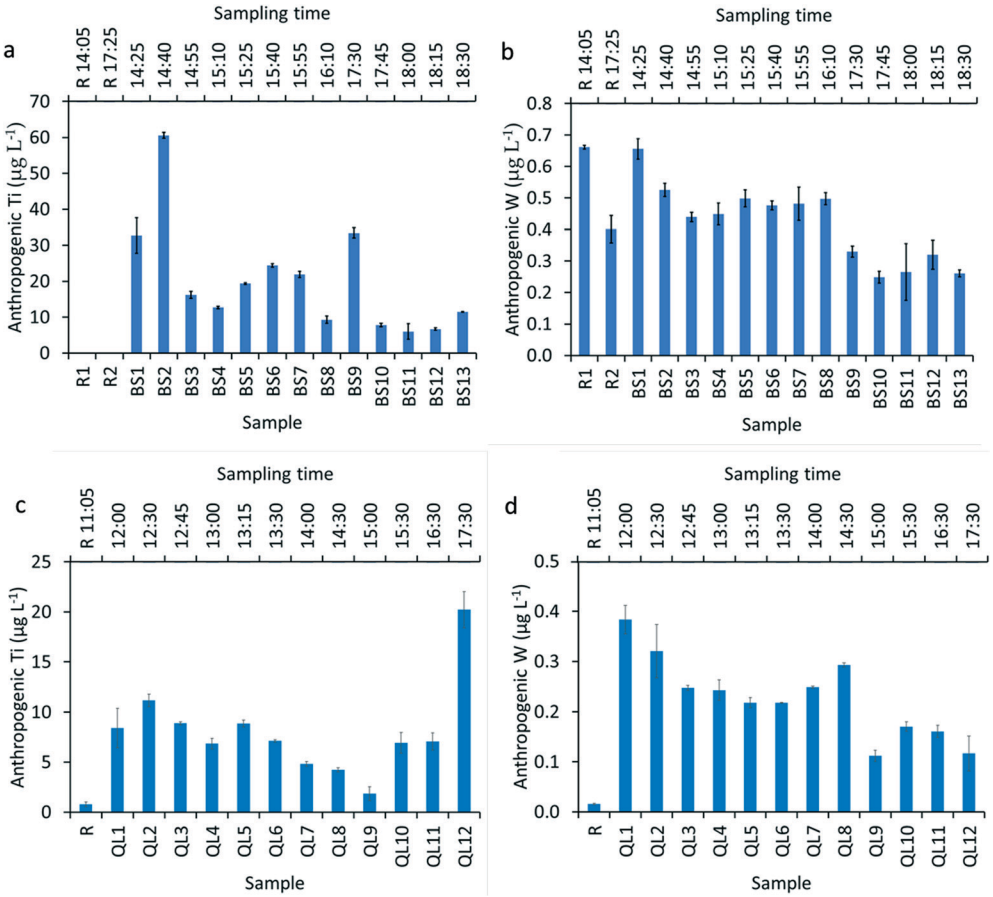

Fig. 7 Concentration of anthropogenic (a and c) Ti and (b and d) W in (a and b) Blossom Street and (c and d) Quail Lane bridge runoff as a function of time following the start of the storm event. R1, R2, and R are rain samples collected at Blossom Street and Quail Lane bridges, respectively. BS1–13 and QL1–12 are bridge runoff samples collected at different time points during rain events (see Table S1).

V, Ni, Bi, W, Pb, and Co).[76,84] Mineralogical analysis of brake pad materials revealed that Fe and graphite are the major common crystalline components. Other mineral species include corundum (Al_2O_3), barite ($BaSO_4$), hematite (Fe_2O_3), metallic Cu, tenorite (CuO) zircon ($ZrSiO_4$), calcite ($CaCO_3$) sulfite species such as stibnite (Sb_2S_3), pyrite (FeS_2), chalcopyrite (ZnS) hauerite (MnS_2) and molybdenite (MoS_2).[76] Brake debris are characterized by elevated concentrations of Fe, Cu, and Ba while tire debris are characterized by elevated concentrations of Zn, Pb, and Cu.[72,73] Additionally, Fe, Cu, Zn, Ni, Cr, Zr, Sn, Cu-bearing NMs were detected in brake wear by scanning electron microscopy coupled with energy dispersive X-ray spectroscopy (EDX).[23,77]

Tungsten -rich NMs could originate from traffic-related emissions as it has many uses in vehicles including in ball joints, brakes, crank shafts in performance vehicles, and other mechanical parts of vehicles that require high wear and/or thermal resistance.[85] For instance, W concentration in brake pad material range from 0 to 9863 mg kg^{-1} with a mean value of 1825 ± 2943 (n = 65) mg kg^{-1}.[84] The elemental associations between W, Mn, Fe, Cu, Sn, and Pb might be due to the use of WC-metal composite high abrasion resistant coatings in brake pads.[86]

Metal and NM concentrations were much higher in the runoff compared to the rain indicating that particles deposited on roads are a major contributor to metal concentrations in runoff. Traffic related metal and NM concentrations (*e.g.*, Cr, Ni, Cu, Mo, Ba, and W; Fig. 1, 2, and 7, Tables S5 and S6†) were higher in Blossom street rain and runoff compared to Quail Lane rain and runoff, likely due to the higher traffic density on Blossom street (AADT = 22 900) compared to Quail Lane (AADT = 1000). Metal and NM concentrations were higher in the Blossom Street rain collected at the peak hour, which can be attributed to increased brake wear emissions. Higher brake wear-related emissions have been reported during rush hour where the traffic often operates in the stop-and-go mode because a higher number of particles are released in the braking phase as compared to the acceleration phase.[87–89]

4. Conclusions

This study illustrated the identification and quantification of various classes of anthropogenic NMs in urban runoff due to mainly non-exhaust traffic-related emissions using a combination of single particle and bulk elemental ratio

analyses. By comparing the relative abundance of smNM and mmNM in urban rain and runoff *vs.* soils, we deduced that the majority of single metal V, Zn, Sn, Sb, Ba, and W NMs can be attributed to anthropogenic inputs. Using SP-ICP-TOF-MS and clustering analysis, multiple anthropogenic NM classes were identified including Ti, W, Fe, Cr, Zn, Cu, Sn, Sb, and V NMs. Using the elemental ratio approach, the total, natural, and anthropogenic Ti and W concentrations were estimated. Estimated anthropogenic Ti concentration in rain was 0.77 ± 0.24 μg L^{-1}, anthropogenic W concentrations in rain ranged from 0.20 ± 0.00 μg L^{-1} to 0.66 ± 0.01 μg L^{-1}. Blossom Street Bridge and Quail Lane Bridge runoff anthropogenic Ti concentrations ranged from 6.0 ± 2.1 μg L^{-1} to 60.6 ± 0.8 μg L^{-1}, and 1.9 ± 0.7 μg L^{-1} to 20.2 ± 1.8 μg L^{-1}, respectively. Blossom Bridge and Quail Bridge runoff anthropogenic W concentrations ranged from 0.23± 0.02 μg L^{-1} to 0.66 ± 0.03 μg L^{-1}, and 0.11± 0.01 μg L^{-1} to 0.38 ± 0.03 μg L^{-1}, respectively.

Anthropogenic metal and NM contamination (*e.g.*, Cr, Ni, Cu, Mo, Ba, and W) increased with traffic density; that is anthropogenic metal and NM concentrations were higher in rain and runoff collected in downtown area (Blossom Street Bridge) compared to rainwater and runoff samples collected in residential area (Quail Lane Bridge). The relative abundance of smNMs, and the number and mass concentration of anthropogenic NMs were also higher in Blossom Street rain and runoff compared to those in Qual Lane rain and runoff due to large size of the bridge and higher traffic. The occurrence of anthropogenic NMs in rain suggests that these NMs were suspended in the atmosphere and thus may pose risk to human health through inhalation. The direct discharge of urban runoff to surface waters implies exposure of aquatic organisms to various anthropogenic NMs, which may pose risk to environmental and human health and warrant further investigations. The mass and number concentrations of anthropogenic NM varied during the sampling period, with highest concentrations occurring at the beginning of the runoff events and increases and decreases throughout the sampling campaigns. This variability in the NM number concentrations might be attributed to sampling time and thus traffic density or to variation in rain intensity. The continuing discharge of anthropogenic NMs in the runoff throughout the rain event indicates a continuous release to environmental systems.

Conflicts of interest

The authors declare no competing interest.

Acknowledgements

This work was supported by US National Science Foundation CAREER (1553909) grant to Dr. Mohammed Baalousha.

Notes and references

1 M. F. Hochella, D. W. Mogk, J. Ranville, I. C. Allen, G. W. Luther, L. C. Marr, B. P. McGrail, M. Murayama, N. P. Qafoku and K. M. Rosso, Natural, incidental, and engineered nanomaterials and their impacts on the Earth system, *Science*, 2019, **363**(6434), eaau8299.

2 J. Wang, M. M. Nabi, S. K. Mohanty, A. N. Afrooz, E. Cantando, N. Aich and M. Baalousha, Detection and quantification of engineered particles in urban runoff, *Chemosphere*, 2020, **248**, 126070.

3 W. Wilczyńska-Michalik, K. Rzeźnikiewicz, B. Pietras and M. Michalik, Fine and ultrafine TiO_2 particles in aerosol in Kraków (Poland), *Mineralogia*, 2015, **45**, 65–77.

4 W. Ouyang, B. Guo, G. Cai, Q. Li, S. Han, B. Liu and X. Liu, The washing effect of precipitation on particulate matter and the pollution dynamics of rainwater in downtown Beijing, *Sci. Total Environ.*, 2015, **505**, 306–314.

5 R. Uchiyama, H. Okochi, N. Katsumi and H. Ogata, The impact of air pollutants on rainwater chemistry during "urban-induced heavy rainfall" in downtown Tokyo, Japan, *J. Geophys. Res.: Atmos.*, 2017, **122**(12), 6502–6519.

6 L. Škrdlíková, L. Landlová, J. Klánová and G. Lammel, Wet deposition and scavenging efficiency of gaseous and particulate phase polycyclic aromatic compounds at a central European suburban site, *Atmos. Environ.*, 2011, **45**(25), 4305–4312.

7 U.S.EPA. Report to Congress on impacts and control of combined sewer overflows and sanitary sewer overflows; EPA 833-R-04-001.

8 Regulations, U. S. E. P. A. O. o. W.; Planning, U. S. E. P. A. O. o. W., National Water Quality Inventory: Report to Congress. Office of Water Regulations and Standards, 1994.

9 H. Jeong, J. Y. Choi, J. Lim, W. J. Shim, Y. O. Kim and K. Ra, Characterization of the contribution of road deposited sediments to the contamination of the close marine environment with trace metals: Case of the port city of Busan (South Korea), *Mar. Pollut. Bull.*, 2020, **161**, 111717.

10 M. M. Nabi, J. Wang and M. Baalousha, Episodic surges in titanium dioxide engineered particle concentrations in surface waters following rainfall events, *Chemosphere*, 2021, **263**, 128261.

11 M. Baalousha, Y. Yang, M. E. Vance, B. P. Colman, S. McNeal, J. Xu, J. Blaszczak, M. Steele, E. Bernhardt and M. F. Hochella Jr, Outdoor urban nanomaterials: The emergence of a new, integrated, and critical field of study, *Sci. Total Environ.*, 2016, **557-558**, 740–753.

12 M. Minguillón, X. Querol, U. Baltensperger and A. Prévôt, Fine and coarse PM composition and sources in rural and urban sites in Switzerland: local or regional pollution?, *Sci. Total Environ.*, 2012, **427**, 191–202.

13 K. M. Conko, K. C. Rice and M. M. Kennedy, Atmospheric wet deposition of trace elements to a suburban environment, Reston, Virginia, USA, *Atmos. Environ.*, 2004, **38**(24), 4025–4033.

14 G. Kim, J. R. Scudlark and T. M. Church, Atmospheric wet deposition of trace elements to Chesapeake and Delaware Bays, *Atmos. Environ.*, 2000, **34**(20), 3437–3444.

15 M. M. Shafer, B. M. Toner, J. T. Overdier, J. J. Schauer, S. C. Fakra, S. Hu, J. D. Herner and A. Ayala, Chemical speciation

of vanadium in particulate matter emitted from diesel vehicles and urban atmospheric aerosols, *Environ. Sci. Technol.*, 2012, **46**(1), 189–195.

16 S. Canepari, C. Perrino, F. Olivieri and M. L. Astolfi, Characterisation of the traffic sources of PM through size-segregated sampling, sequential leaching and ICP analysis, *Atmos. Environ.*, 2008, **42**(35), 8161–8175.

17 K. Cheung, L. Ntziachristos, T. Tzamkiozis, J. Schauer, Z. Samaras, K. Moore and C. Sioutas, Emissions of particulate trace elements, metals and organic species from gasoline, diesel, and biodiesel passenger vehicles and their relation to oxidative potential, *Aerosol Sci. Technol.*, 2010, **44**(7), 500–513.

18 A. Thorpe and R. M. Harrison, Sources and properties of non-exhaust particulate matter from road traffic: A review, *Sci. Total Environ.*, 2008, **400**(1–3), 270–282.

19 J. K. Gietl, R. Lawrence, A. J. Thorpe and R. M. Harrison, Identification of brake wear particles and derivation of a quantitative tracer for brake dust at a major road, *Atmos. Environ.*, 2010, **44**(2), 141–146.

20 P. Wåhlin, R. Berkowicz and F. Palmgren, Characterisation of traffic-generated particulate matter in Copenhagen, *Atmos. Environ.*, 2006, **40**(12), 2151–2159.

21 P. Pant and R. M. Harrison, Estimation of the contribution of road traffic emissions to particulate matter concentrations from field measurements: A review, *Atmos. Environ.*, 2013, **77**, 78–97.

22 T. B. Councell, K. U. Duckenfield, E. R. Landa and E. Callender, Tire-Wear Particles as a Source of Zinc to the Environment, *Environ. Sci. Technol.*, 2004, **38**(15), 4206–4214.

23 K. Adachi and Y. Tainosho, Characterization of heavy metal particles embedded in tire dust, *Environ. Int.*, 2004, **30**(8), 1009–1017.

24 S. Venkatesan and P. Kadiresh, Influence of an aqueous cerium oxide nanofluid fuel additive on performance and emission characteristics of a compression ignition engine, *Int. J. Ambient Energy*, 2016, **37**(1), 64–67.

25 E. Aneggi, C. de Leitenburg, M. Boaro, P. Fornasiero and A. Trovarelli, *Catalytic applications of cerium dioxide. In Cerium Oxide (CeO_2): Synthesis, Properties and Applications*, Elsevier, 2020, pp. 45–108.

26 K. Kannaiyan and R. Sadr, The effects of alumina nanoparticles as fuel additives on the spray characteristics of gas-to-liquid jet fuels, *Exp. Therm. Fluid Sci.*, 2017, **87**, 93–103.

27 D. Ganesh and G. Gowrishankar, in *Effect of nano-fuel additive on emission reduction in a biodiesel fuelled CI engine, 2011 International conference on electrical and control engineering*, IEEE, 2011, pp. 3453–3459.

28 G. V. Research, Traffic Road Marking Coatings Market Size, Share & Trends Analysis Report By Product (Paint, Thermoplastic, Preformed Polymer Tape), By Type (Permanent, Removable), By Application, By Region, And Segment Forecasts, 2020–2027. https://www.grandviewresearch.com/industry-analysis/traffic-road-marking-coatings-market/request. Grand View Research, 2020.

29 M. Baalousha, J. Wang, M. M. Nabi, F. Loosli, R. Valenca, S. K. Mohanty, N. Afrooz, E. Cantando and N. Aich, Stormwater green infrastructures retain high concentrations of TiO2 engineered (nano)-particles, *J. Hazard. Mater.*, 2020, **392**, 122335.

30 T. Grigoratos and G. Martini, Brake wear particle emissions: a review, *Environ. Sci. Pollut. Res.*, 2015, **22**(4), 2491–2504.

31 M. Rexeis and S. Hausberger, Trend of vehicle emission levels until 2020–Prognosis based on current vehicle measurements and future emission legislation, *Atmos. Environ.*, 2009, **43**(31), 4689–4698.

32 C. C. Lin, S. J. Chen, K. L. Huang, W. I. Hwang, G. P. Chang-Chien and W. Y. Lin, *Characteristics of Metals in Nano/Ultrafine/Fine/Coarse Particles Collected Beside a Heavily Trafficked Road. In Environ. Sci. Technol. Environmental Science & Technology*, American Chemical Society, 2005, vol. 39, pp. 8113–8122.

33 G. M. Lovett, M. M. Traynor, R. V. Pouyat, M. M. Carreiro, W.-X. Zhu and J. W. Baxter, Atmospheric deposition to oak forests along an urban– rural gradient, *Environ. Sci. Technol.*, 2000, **34**(20), 4294–4300.

34 J. Sansalone and S. Buchberger, *Partitioning and First Flush of Metals in Urban Roadway Storm Water. In J. Environ. Eng Journal of Environmental Engineering*, American Society of Civil Engineers, 1997, vol. 123, pp. 134–143.

35 A. P. Davis, M. Shokouhian and S. Ni, Loading estimates of lead, copper, cadmium, and zinc in urban runoff from specific sources, *Chemosphere*, 2001, **44**(5), 997–1009.

36 J. Buffle and H. Van Leeuwen, *Environmental particles*, Lewis, Boca Raton, FL, 1992, vol. 1.

37 F. Gottschalk, T. Sonderer, R. W. Scholz and B. Nowack, Modeled Environmental Concentrations of Engineered Nanomaterials (TiO2, ZnO, Ag, CNT, Fullerenes) for Different Regions, *Environ. Sci. Technol.*, 2009, **43**(24), 9216–9222.

38 F. Gottschalk, T. Sun and B. Nowack, Environmental concentrations of engineered nanomaterials: Review of modeling and analytical studies, *Environ. Pollut.*, 2013, **181**(0), 287–300.

39 M. M. Nabi, J. Wang, M. Meyer, M.-N. Croteau, N. Ismail and M. Baalousha, Concentrations and size distribution of TiO2 and Ag engineered particles in five wastewater treatment plants in the United States, *Sci. Total Environ.*, 2021, **753**, 142017.

40 F. Loosli, J. Wang, S. Rothenberg, M. Bizimis, C. Winkler, O. Borovinskaya, L. Flamigni and M. Baalousha, Sewage spills are a major source of titanium dioxide engineered (nano)-particle release into the environment, *Environ. Sci.: Nano*, 2019, **6**(3), 763–777.

41 A. Praetorius, A. Gundlach-Graham, E. Goldberg, W. Fabienke, J. Navratilova, A. Gondikas, R. Kaegi, D. Günther, T. Hofmann and F. von der Kammer, Single-particle multi-element fingerprinting (spMEF) using inductively-coupled plasma time-of-flight mass spectrometry (ICP-TOFMS) to identify engineered nanoparticles against the elevated natural background in soils, *Environ. Sci.: Nano*, 2017, **4**(2), 307–314.

42 F. Loosli, Z. Yi, J. Wang and M. Baalousha, Improved extraction efficiency of natural nanomaterials in soils to facilitate their characterization using a multimethod approach, *Sci. Total Environ.*, 2019, **677**, 34–46.
43 S. Rodrigues, G. D. Bland, X. Gao, S. M. Rodrigues and G. V. Lowry, Investigation of pore water and soil extraction tests for characterizing the fate of poorly soluble metal-oxide nanoparticles, *Chemosphere*, 2021, **267**, 128885.
44 L. G. Jahn, G. D. Bland, L. W. Monroe, R. C. Sullivan and M. E. Meyer, Single-particle elemental analysis of vacuum bag dust samples collected from the International Space Station by SEM/EDX and sp-ICP-ToF-MS, *Aerosol Sci. Technol.*, 2021, **55**(5), 571–585.
45 A. Gondikas, F. von der Kammer, R. Kaegi, O. Borovinskaya, E. Neubauer, J. Navratilova, A. Praetorius, G. Cornelis and T. Hofmann, Where is the nano? Analytical approaches for the detection and quantification of TiO 2 engineered nanoparticles in surface waters, *Environ. Sci.: Nano*, 2018, **5**(2), 313–326.
46 K. Mehrabi, R. Kaegi, D. Günther and A. Gundlach-Graham, Emerging investigator series: automated single-nanoparticle quantification and classification: a holistic study of particles into and out of wastewater treatment plants in Switzerland, *Environ. Sci.: Nano*, 2021, **8**, 1211.
47 SCDOT, 2019 sverage daily traffic for dorchester county. https://www.scdot.org/travel/pdf/trafficcounts/2019/Dorchester.pdf. SCDOT Road Data Services, 2021.
48 M. Baalousha, J. Wang, M. Erfani and E. Goharian, Elemental fingerprints in natural nanomaterials determined using SP-ICP-TOF-MS and clustering analysis, *Sci. Total Environ.*, 2021, **792**, 148426.
49 L. Hendriks, A. Gundlach-Graham, B. Hattendorf and D. Günther, Characterization of a new ICP-TOFMS instrument with continuous and discrete introduction of solutions, *J. Anal. At. Spectrom.*, 2017, **32**(3), 548–561.
50 H. E. Pace, N. J. Rogers, C. Jarolimek, V. A. Coleman, C. P. Higgins and J. F. Ranville, Determining transport efficiency for the purpose of counting and sizing nanoparticles via single particle inductively coupled plasma mass spectrometry, *Anal. Chem.*, 2011, **83**(24), 9361–9369.
51 M. Tanner, Shorter signals for improved signal to noise ratio, the influence of Poisson distribution, *J. Anal. At. Spectrom.*, 2010, **25**(3), 405–407.
52 F. Nielsen, *Introduction to HPC with MPI for Data Science*, Springer, 2016.
53 P. Noll Jr, H. Newsom, W. Leeman and J. G. Ryan, The role of hydrothermal fluids in the production of subduction zone magmas: evidence from siderophile and chalcophile trace elements and boron, *Geochim. Cosmochim. Acta*, 1996, **60**(4), 587–611.
54 K. Sims, H. Newsom and E. Gladney, Chemical fractionation during formation of the Earth's core and continental crust: clues from As, Sb, W, and Mo, *Origin of the Earth*, 1990, 291–317.
55 H. Newsom, W. White, K. Jochum and A. Hofmann, Siderophile and chalcophile element abundances in oceanic basalts, Pb isotope evolution and growth of the Earth's core, *Earth Planet. Sci. Lett.*, 1986, **80**(3–4), 299–313.
56 H. E. Newsom and H. Palme, The depletion of siderophile elements in the Earth's mantle: new evidence from molybdenum and tungsten, *Earth Planet. Sci. Lett.*, 1984, **69**(2), 354–364.
57 H. E. Newsom, K. W. Sims, P. D. Noll Jr, W. L. Jaeger, S. A. Maehr and T. B. Beserra, The depletion of tungsten in the bulk silicate earth: constraints on core formation, *Geochim. Cosmochim. Acta*, 1996, **60**(7), 1155–1169.
58 R. Arevalo Jr and W. F. McDonough, Tungsten geochemistry and implications for understanding the Earth's interior, *Earth Planet. Sci. Lett.*, 2008, **272**(3–4), 656–665.
59 D. B. C. Smith, W. F. Woodruff, L. G. Solano, F. Ellefsen and J. Karl, *Geochemical and mineralogical maps for soils of the conterminous United States*, 2014.
60 G. P. Hu, R. Balasubramanian and C. D. Wu, Chemical characterization of rainwater at Singapore, *Chemosphere*, 2003, **51**(8), 747–755.
61 H. Hou, T. Takamatsu, M. Koshikawa and M. Hosomi, Trace metals in bulk precipitation and throughfall in a suburban area of Japan, *Atmos. Environ.*, 2005, **39**(20), 3583–3595.
62 J. Hamilto-Taylor and M. Willis, A quantitative assessment of the sources and general dynamics of trace metals in a soft-water lake, *Limnol. Oceanogr.*, 1990, **35**(4), 840–851.
63 S. Jonnalagadda, J. Makadho, N. Matinde, R. Karimanzira and A. Makarau, Chemical composition of rainwater and air quality in Zimbabwe, Africa, *Sci. Total Environ.*, 1994, **144**(1–3), 261–271.
64 R. Rudnick, S. Gao, H. Holland and K. Turekian, Composition of the continental crust, *The crust*, 2003, **3**, 1–64.
65 W. He, I. O. Wallinder and C. Leygraf, A laboratory study of copper and zinc runoff during first flush and steady-state conditions, *Corros. Sci.*, 2001, **43**(1), 127–146.
66 D. Wilson, *Highway 520 Bridge Storm Water Runoff Study. King County Water and Land Resources Division*, Department of Natural Resources and Parks, Seattle, WA, USA, 2006, pp. 1–66.
67 S. Azimi, V. Rocher, M. Muller, R. Moilleron and D. R. Thevenot, Sources, distribution and variability of hydrocarbons and metals in atmospheric deposition in an urban area (Paris, France), *Sci. Total Environ.*, 2005, **337**(1–3), 223–239.
68 A. Borawski, Conventional and unconventional materials used in the production of brake pads–review, *Sci. Eng. Compos. Mater.*, 2020, **27**(1), 374–396.
69 R. Huston, Y. Chan, T. Gardner, G. Shaw and H. Chapman, Characterisation of atmospheric deposition as a source of contaminants in urban rainwater tanks, *Water Res.*, 2009, **43**(6), 1630–1640.
70 E. A. Smail, E. A. Webb, R. P. Franks, K. W. Bruland and S. A. Sañudo-Wilhelmy, Status of metal contamination in surface waters of the coastal ocean off Los Angeles, California since the implementation of the Clean Water Act, *Environ. Sci. Technol.*, 2012, **46**(8), 4304–4311.

71 M. Huber, A. Welker and B. Helmreich, Critical review of heavy metal pollution of traffic area runoff: Occurrence, influencing factors, and partitioning, *Sci. Total Environ.*, 2016, **541**, 895–919.
72 E. R. McKenzie, J. E. Money, P. G. Green and T. M. Young, Metals associated with stormwater-relevant brake and tire samples, *Sci. Total Environ.*, 2009, **407**(22), 5855–5860.
73 M. Legret and C. Pagotto, Evaluation of pollutant loadings in the runoff waters from a major rural highway, *Sci. Total Environ.*, 1999, **235**(1–3), 143–150.
74 X. Huang, I. Olmez, N. K. Aras and G. E. Gordon, Emissions of trace elements from motor vehicles: potential marker elements and source composition profile, *Atmos. Environ.*, 1994, **28**(8), 1385–1391.
75 H. Lipowsky and E. Arpaci, *Copper in the automotive industry*, John Wiley & Sons, 2008.
76 F. Amato, O. Font, N. Moreno, A. Alastuey and X. Querol, Mineralogy and elemental composition of brake pads of common use in Spain, *Macla*, 2012, **16**, 154–156.
77 C. Gunawardana, A. Goonetilleke, P. Egodawatta, L. Dawes and S. Kokot, Source characterisation of road dust based on chemical and mineralogical composition, *Chemosphere*, 2012, **87**(2), 163–170.
78 H. Yan, H. Bi, X. Li and Z. Xu, Precipitation and mechanical properties of Nb-modified ferritic stainless steel during isothermal aging, *Mater. Charact.*, 2009, **60**(3), 204–209.
79 N. D. Nam and J. G. Kim, Effect of niobium on the corrosion behaviour of low alloy steel in sulfuric acid solution, *Corros. Sci.*, 2010, **52**(10), 3377–3384.
80 S. Rahimpour Golroudbary, N. Krekhovetckii, M. El Wali and A. Kraslawski, Environmental sustainability of niobium recycling: the case of the automotive industry, *Recycling*, 2019, **4**(1), 5.
81 S. Shanmugam, R. D. K. Misra, J. Hartmann and S. G. Jansto, Microstructure of high strength niobium-containing pipeline steel, *Mater. Sci. Eng., A*, 2006, **441**(1), 215–229.
82 A. Hegetschweiler, O. Borovinskaya, T. Staudt and T. Kraus, Single-Particle Mass Spectrometry of Titanium and Niobium Carbonitride Precipitates in Steels, *Anal. Chem.*, 2019, **91**(1), 943–950.
83 J. Pey, X. Querol and A. Alastuey, Discriminating the regional and urban contributions in the North-Western Mediterranean: PM levels and composition, *Atmos. Environ.*, 2010, **44**(13), 1587–1596.
84 J. H. J. Hulskotte, G. D. Roskam and H. A. C. Denier van der Gon, Elemental composition of current automotive braking materials and derived air emission factors, *Atmos. Environ.*, 2014, **99**, 436–445.
85 Carbide-USA, *The Use of Tungsten Carbide in the Automotive Industry*, https://www.carbide-usa.com/use-tungsten-carbide-automotive-industry/, 2021, (date accessed 05/10/2022).
86 O. Aranke, W. Algenaid, S. Awe and S. Joshi, Coatings for automotive gray cast iron brake discs: A review, *Coatings*, 2019, **9**(9), 552.
87 A. P. Grieshop, E. M. Lipsky, N. J. Pekney, S. Takahama and A. L. Robinson, Fine particle emission factors from vehicles in a highway tunnel: Effects of fleet composition and season, *Atmos. Environ.*, 2006, **40**, 287–298.
88 T. Hussein, C. Johansson, H. Karlsson and H.-C. Hansson, Factors affecting non-tailpipe aerosol particle emissions from paved roads: On-road measurements in Stockholm, Sweden, *Atmos. Environ.*, 2008, **42**(4), 688–702.
89 M. Mathissen, V. Scheer, R. Vogt and T. Benter, Investigation on the potential generation of ultrafine particles from the tire–road interface, *Atmos. Environ.*, 2011, **45**(34), 6172–6179.